Chapter 10
Design and Calibration Strategies for Improving HCCI Combustion in Dual-Fuel Diesel–Methane Engines

A. P. Carlucci, A. Ficarella, D. Laforgia and L. Strafella

Abstract The interest in methane is lately increased due to power-to-gas technologies, through which green electricity in excess could be used to produce easily storable gaseous fuels. Among engines for methane exploitation, dual-fuel piston engine is a very efficient and low-impact solution. Their operation, still limited by high hydrocarbons and carbon monoxide emissions at low loads and knock at high loads, is characterized by many parameters. Besides the ones well recognized in the literature, like pilot quantity and substitution rate, other parameters, like engine volumetric compression ratio, intake charge conditions, pilot injection pressure and timing, engine load and speed, and exhaust gas recirculation (EGR), showed an impact on engine performance and emissions. This work first describes the results of a full factorial DoE in which the effects of compression ratio, intake charge pressure (ICP), pilot injection timing and pressure, and methane flow rate effect are evaluated and discussed on combustion development, engine performance, and pollutant emission levels at the exhaust. Through analysis of variance (ANOVA), the first- and second-order effects were also quantified. Moreover, the factor variation ranges leading the engine to operate in or close to HCCI combustion, i.e., guaranteeing a high conversion efficiency and low emission levels at the same time, were sought and highlighted. This suggested that not only very advanced but also retarded injection timings, combined with high ICP, determine very low levels of nitrogen oxides and maximum pressure rise rate, with little or no penalty on engine efficiency and emission levels.

Keywords Dual fuel · Diesel fuel · Methane · Injection pressure
Injection timing · Volumetric compression ratio · Methane flow rate
Intake charge pressure · HCCI combustion · MK combustion · ANOVA

A. P. Carlucci (✉) · A. Ficarella · D. Laforgia · L. Strafella
Department of Engineering for Innovation (DII), University of Salento, via per Monteroni, 73100 Lecce, Italy
e-mail: paolo.carlucci@unisalento.it

K. K. Srinivasan et al. (eds.), *Natural Gas Engines*, Energy, Environment, and Sustainability, https://doi.org/10.1007/978-981-13-3307-1_10

10.1 Introduction

Among all alternative fuels, methane or natural gas (NG, whose main constituent is methane) has been considered since a long time among the best solutions for fossil fuel substitution because of their availability throughout the world, inherent clean burning, favorability as fuels, and adaptability to piston (compression or spark ignition) engines in addition to turbine engines (Muhammad et al. 2016; Pali et al. 2018). The interest in natural gas is lately increased due to power-to-gas technologies, through which green electricity in excess could be used to produce easily storable gaseous fuels (McKennaa et al. 2018; He et al. 2018). Focusing the attention on piston engines, it is worth mentioning that existing engines, both spark and compression ignition, can be readily converted to operate primarily on methane or NG, with the latter preferred to the former since characterized by a higher compression ratio and therefore lower fuel consumption. In this case, however, diesel (or a high reactivity fuel) must be used as a spark plug to achieve ignition, given the lower reactivity of methane; this kind of engines is referred to as "dual fuel" (DF). The substitution rates of the high reactivity fuel with a low reactivity one can overcome 90% in the currently available dual-fuel engines, so significantly reducing CO_2 and particulate matter (PM) emission levels. However, besides the advantages of dual-fuel combustion, some well-known drawbacks also arise, as the knock tendency at high loads and excessive total hydrocarbons (THCs) and carbon monoxide (CO) production at low loads.

Homogeneous charge compression ignition (HCCI) combustion can be a viable solution to drastically reduce these problems (Hasan and Rahman 2016). In HCCI operation—probably the first low-temperature combustion (LTC) mode introduced—air and fuel are homogeneously mixed before being ignited through compression. In this way, fuel-rich zones are avoided, local temperatures are reduced, and, overall, emissions are drastically decreased. In dual-fuel diesel–methane engines, as previously said, the ignition of a mixture of air and methane is obtained thanks to an injection of diesel fuel. Implementing HCCI in dual-fuel diesel–methane engines, therefore, requires to obtain a homogeneous mixture of air and methane as well as homogeneous distribution of diesel fuel vapor inside the cylinder before the start of ignition. While mixing homogeneously air and methane is a relatively easy task, the same cannot be said about diesel fuel. Several attempts have been documented in which the diesel fuel is fumigated along the intake duct. However, this solution, while guaranteeing a proper homogenization of the diesel fuel with air before ignition, presents as drawbacks the high PM emission levels due to poor fuel atomization conditions (Song et al. 2018).

Therefore, it is usually preferred to increase the ignition delay of the mixture, so giving more time to diesel fuel to evaporate and mix with the air. In this way, however, a perfect homogeneity is generally not obtained. The so-called partially premixed compression ignition (PPCI) or predominantly premixed charge compression ignition (PPCCI) combustion is achieved with direct injection system, where advanced multi-injection strategies lead to a certain degree of premixing of

fuel and air, although not definable as HCCI. On the other hand, the so-called reactivity-controlled compression ignition (RCCI) combustion, developed to control fuel reactivity to optimize combustion phasing, duration, and magnitude, is usually implemented in dual-fuel engines performing a very advanced pilot injection. In the open literature, the effect of the different parameters, like pilot start of injection (SOI), pilot injection pressure (p_rail), pilot injection splitting, substitution rate, engine compression ratio (CR), intake charge pressure (ICP) and temperature (ICT), exhaust gas recirculation (EGR), and pilot fuel chemical composition, was evaluated with the goal of increasing the mixture ignition delay in dual-fuel conditions.

In Guerry et al. (2016), the authors varied SOI on a wide range of values, testing a single-cylinder compression ignition engine, observing that, when SOI was advanced, the ignition delay (ID) and the separation between the end of injection and start of combustion both increased; the heat release rate (HRR) curve changed from a distinct two-stage profile to a smooth single-stage profile. Correspondingly, the fuel conversion efficiency η_f increased together with cycle-to-cycle variability and THC and CO emission levels, while NO_x and smoke were reduced drastically. Similar results on a six-cylinder engine were reported in Doosje (2014).

In Raihan et al. (2015), the authors extended the experimental campaign reported in Guerry et al. (2016) and underlined that LTC can be established in a diesel-ignited methane dual-fuel engine setting appropriate values of SOI, p_rail, and ICP.

In Ibrahim et al. (2015), the authors, testing a single-cylinder compression ignition engine operated in dual-fuel diesel–biogas mode, demonstrated that, acting on SOI, ICT, and substitution rate, the engine could be effectively operated in PPCCI at low/medium loads with beneficial reduction of nitric oxides (NO_x) and THC with respect to conventional DF combustion mode.

Srinivasan et al. (2006) studied early pilot injection strategy on a single-cylinder diesel–methane engine and discussed the effect of pilot-injected quantity and ICT on the onset of ignition and combustion.

A comprehensive work is illustrated in Napolitano et al. (2017), Di Blasio et al. (2017a, b), where the authors, testing a single-cylinder representing the technology of a modern light-duty engine operated in DF diesel–methane mode, found that CR is an important engine design parameter, which has a relevant effect on methanic THC emissions. Its effect, however, is more evident at low/medium load. A CR value of 15.5 led to the best performance in terms of pollutant emissions and CO_2 saving over the New European Driving Cycle (NEDC), a test cycle. Other technologies, like double-pulse injection strategy, air throttling, and EGR, were found effective too in controlling pollutant emission levels while respecting engine functional limits, like maximum pressure rise rate (MPRR), cycle-to-cycle variability, and peak firing pressure. However, the investigated parameters were varied in a limited range of values, so that no alternative combustions like HCCI or PPCCI were observed. A similar work, limited to SOI and p_rail varied on a range of conventional values, led to similar results (Yang et al. 2015). In Dahodwala et al.

(2014), the authors, exploiting an optimization routine in which strategies were developed primarily involving diesel SOI and NG substitution rate, demonstrated that it was possible to achieve an average of 49% substitution across the test point map of six-cylinder engine with 15% reduction in NO_x and 43% reduction in PM emissions. At higher engine speeds, it appears that reduced time for CNG/air mixing results in a varying cylinder-to-cylinder distribution of CNG and thus deteriorated combustion stability. RCCI combustion could be achieved at low loads, which enabled even higher NG substitution and lower emissions. A maximum of 50% net indicated thermal efficiency was observed at 6 bar of brake mean effective pressure (BMEP) load point along with 75% reduction in both NO_x and PM emissions. The potential benefits of RCCI combustion were limited due to the un-optimized combustion chamber design and high compression ratio.

The effect of pilot injection pressure, p_rail, has been extensively studied, for example, in Hariprasad (2013). A dual-fuel single-cylinder engine was found to run smoothly with higher injector opening pressure and advanced SOI. The efficiency of the dual-fuel engine is slightly less as compared to neat diesel operation at part loads. The dual-fuel engine resulted in lower smoke and NO_x emissions as compared to neat diesel operation, but it emitted slightly higher CO and THC emissions.

Ryu (2013a, b) studied the NG dual-fuel combustion varying SOI in the range 11–23 crank angle degrees before top dead center (CAD BTDC) and p_rail from 30 to 150 MPa and concluded that: (1) The increase of pilot injection pressure results in lower smoke, but higher NO_x emission; (2) smoke is decreased, and NO_x is increased as the pilot injection timing is advanced; compared to diesel-only combustion, however, smoke emissions are significantly reduced over the range of operating conditions and NO_x emissions are also decreased over the range with the exception of the full load case.

In Xu et al. (2016a, b), a comprehensive study has been performed in which the pilot fuel has been injected shifted in a pre and a pilot or main injections on a very wide range of values, and the effect of p_rail and SOI on combustion and emission of a six-cylinder dual-fuel engine has been assessed. Results indicate that early pre-injection mode leads to lower cylinder pressure and HRR due to a decrease of combustion intensity; thereby, lower NO_x emission is obtained. In contrast, close pre-injection timing leads to large strengthening in combustion which is not beneficial for improving NO_x emission performance. Increase of pre-injection quantity ratio leads to the delayed start of combustion and slower burning rate, and thereby lower NO_x and higher THC emission. However, too high pre-injection quantity ratio leads to unstable combustion. Increasing p_rail leads to rapid combustion and therefore higher cylinder pressure and HRR. Consequently, in-cylinder combustion temperature increases, NO_x emission increases, and THC emission decreases.

In Ogawa et al. (2016), the authors demonstrated that, increasing the injection pressure of diesel fuel, the combustion efficiency increases with a decrease of THC and CO emissions, and the indicated thermal efficiency improves without an increase in NO_x emissions. Simultaneous reductions in the NO_x, THC, and CO emissions can be established with maintaining the equivalence ratio of NG with intake gas throttling under the 250 MPa pilot injection condition. Two-stage split

pilot injection of diesel fuel significantly reduces the maximum rate of pressure rise and NO_x emissions without deteriorations in both thermal efficiency and emissions. In Garcia and Tunestal (2015), the injection strategy, in terms of a number of injections and their timing, was varied in order to establish different combustion modes (namely conventional dual fuel, PPCI, and RCCI) on a dual-fuel methane–diesel engine. In Ansari et al. (2016), it was shown that low reactive mixture outside of the bowl at single-injection strategy showed to be the main reason for the high THC and CO at low loads. Dual-injection strategy provided a high reactive mixture inside and outside of the bowl, resulting in low CO and THC emissions.

Paykani et al. (2015) developed a simulation study on the combustion and emission performance of natural gas/diesel RCCI combustion varying SOI and pilot injection quantity in the presence of split fuel injection strategy. The results demonstrate that: (1) SOI timing of the first injection increases mixture stratification as retarded toward top dead center (TDC), and, as a result, combustion phasing is advanced and soot and NO_x increased; (2) the effect of SOI of second injection is similar to the first one, but only up to a certain point (−30 after TDC, ATDC); (3) as the amount of diesel fuel injected in the second injection is increased, so is the mixture stratification, with the results already illustrated on soot and NO_x; (4) increasing ICT, reaction rates increase, which increase NO_x and advance combustion phasing, while combustion efficiency is reduced because of lower volumetric efficiency; (5) with the explored injection strategies, NO_x and soot can be controlled, while CO and THC deteriorate.

Results of a numerical investigation are also reported in Poorghasemi et al. (2017), where the effect of diesel injection strategies, injection pressure, and spray angle on an RCCI engine performance and emission characteristics was investigated. Concerning injection strategies, results confirmed those reported in Paykani et al. (2015). Moreover, it was demonstrated that higher p_rail increases the spray penetration (causing wall impingement) as well as evaporation rate of diesel droplets: In this way, stratification of diesel fuel increases and combustion phasing is advanced. As a consequence, NO_x, THC, and CO all increase. A narrower spray angle determines higher values of THC and CO emissions near the cylinder wall and crevice volumes, and NO_x increases due to richer and locally higher reactive zone with higher combustion temperature. These findings have been confirmed by imaging techniques (Nithyanandan et al. 2017).

Several numerical works (Wang et al. 2016; Donateo et al. 2014) have proven the possibility to decrease both CO and THC emissions properly designing combustion chamber geometry, spray pattern, and SOI.

Finally, several benefits on DF PPCCI deriving from using biodiesel fuels were highlighted in Gharehghani et al. (2015), Hosmath et al. (2016). In Hosmath et al. (2016), the effect of CR, NG flow rate, and SOI has been analyzed on the performance of a dual-fuel engine operated on Honge oil methyl ester (HOME) and NG applying response surface methodology on the results of an experimental campaign.

As evident from the review of the open literature, a significant research activity has been performed on dual-fuel diesel–methane combustion, aiming at improving

the engine performance and reducing its environmental impact but acting on one or few controlling factors at a time. Therefore, the aim of this work is to identify the engine design and management factors—characterizing the dual-fuel combustion—most influential on engine operation outputs. In order to perform this analysis, a set of factors, namely methane flow rate, pilot injection pressure, pilot injection timing, engine volumetric compression ratio, and ICP, have been varied on different levels during an extensive experimental campaign. Their effect on engine output parameters, namely indicated mean effective pressure (IMEP), fuel conversion efficiency η_f, combustion start, position and duration, maximum pressure rise rate (MPRR), NO_x, THC, and CO emission levels, has been analyzed using an analysis of variance (ANOVA) approach. In this way, it was possible to recognize the factor (or combination of factors) most influential on each engine output parameter. Moreover, the factor variation ranges leading the engine to operate in or close to HCCI combustion, i.e., guaranteeing a high conversion efficiency and low emission levels at the same time, have been sought: this suggested alternative and potentially more effective ways to operate the engine closer to HCCI conditions.

10.2 Experimental Layout

A single-cylinder, 4-stroke, common rail diesel research engine (AVL model 5402) was used to analyze the effect of pilot injection pressure and timing, engine compression ratio, intake air pressure, and methane amount on dual-fuel diesel fuel–methane performance and emissions. The technical features of the engine are reported in Table 10.1, while in Fig. 10.1 the scheme of the experimental layout is reported. The gaseous methane has been fumigated along the intake duct of the engine by means of an injector consisting of an automatic poppet valve, with contrast spring, actuated by the methane itself introduced by a solenoid valve in a small accumulation volume (Carlucci et al. 2008). The solenoid valve was actuated using a duty cycle $D = 50\%$ with a frequency of 30 Hz. During the tests, the injector was positioned at a distance of about 400 mm from the cylinder axis, so that a homogeneous methane–air mixture was obtained before trapping it into the cylinder. Although the engine is provided with a swirl and tumble valve, the mixture was introduced in the cylinder through the swirl valve only. This solution was chosen because it provided the best compromise in terms of engine performance and emission levels (Carlucci et al. 2009, 2010).

Table 10.2 reports the levels assigned to each factor varied during tests. The duration of the diesel fuel injection was adjusted in order to keep constant—equal to 6 mm^3/cycle—the diesel fuel amount injected per cycle. In particular, duration equal to 150 or 300 μs was set for a diesel fuel injection pressure (p_rail), respectively, equal to 1250 or 500 bar. The engine was always run at 1500 rpm. Referring to SOI variation range, more advanced SOI was not used because of either the high MPRR observed in several conditions, not tolerable by the engine structure, or the absence of combustion observed in several other conditions. On the

Table 10.1 Single-cylinder diesel engine main specifications

Specification	Nominal value/description	
Maximum power	18 kW	
Bore	85 mm	
Stroke	90 mm	
Original compression ratio	17.1:1	
Combustion chamber	Bowl with valve pockets and flathead	
Injection system	Common rail	
Max injection pressure	1300 bar	
Valve timing	Opening	Closing
Intake	13.5° BTDC	46.5° ABDC
Exhaust	51.5° BBDC	16.5° ATDC

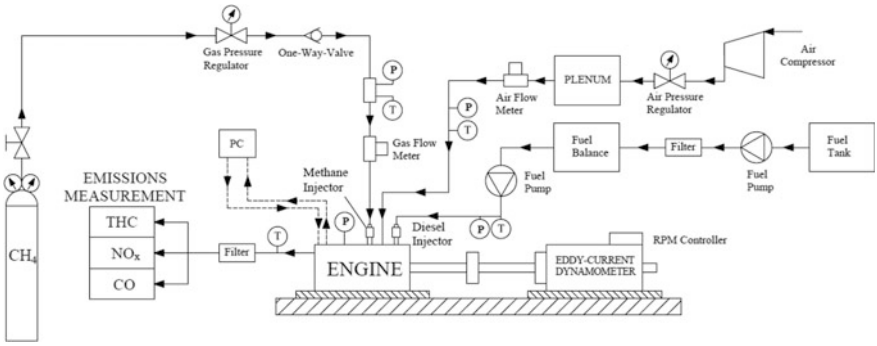

Fig. 10.1 Experimental setup

Table 10.2 Factors and corresponding levels varied during tests

Description	Abbreviation	Tested levels
Methane mass flow rate	G_{gas}	0 (kg/h)—(IMEP ≈ 0.8 bar) 0.21 (kg/h)—(IMEP ≈ 1.3 bar) 0.31 (kg/h)—(IMEP ≈ 2.4 bar) 0.37 (kg/h)—(IMEP ≈ 4 bar) 0.40 (kg/h)—(IMEP ≈ 6 bar)
Engine compression ratio	CR	14–17
Intake charge pressure	ICP	1.16–1.66 (bar)
Diesel fuel injection pressure	p_rail	500–1250 (bar)
Diesel fuel pilot injection timing	SOI	−50/−35/−20/−10/0/5/10 (CAD ATDC)

other hand, results obtained with more retarded SOI are not shown as the combustion was basically not observed.

The amount of methane introduced along the intake duct was varied acting on the duty cycle of a continuous pulse-width modulation (PWM) signal, generated by

a National Instruments High-Speed, Sourcing Digital Output NI 9474 module and controlled by means of LabVIEW software. In this way, the opening time of the gas injector was varied and so the amount of adducted methane.

The engine compression ratio was varied by changing the dead space volume of the engine. In particular, thanks to the modular composition of the engine, steel plates of a specific thickness can be inserted or removed to vary the compression ratio.

The ICP was varied by modifying the opening of a pressure-regulating valve positioned on the outflow line of an ATLAS COPCO GA 30 compressor. Also, in this case, modifying the duty cycle of a PWM signal, it was possible to modify the valve-opening degree and therefore the ICP up to the desired value. The intake charge temperature (ICT) was kept constant equal to 314 ± 2 K.

Data acquisition was started only after steady conditions were reached. An AVL piezoelectric pressure sensor model QC33C was mounted in the combustion chamber. The signal sampling was triggered and synchronized with TDC by an AVL encoder model 364C with a resolution of 0.2 crank angle degree (CAD). The in-cylinder pressure transducer was characterized by a linearity error lower than 0.4%, while the sensitivity shift and the range error of the pressure amplifier (AVL model 3066A01) were less than 1%. The error associated with the A/D data conversion and acquisition was equal to 0.3%. To obtain the absolute cylinder pressure, ($p_{\mathrm{cyl,abs}}$), a pegging routine was implemented, through which the cylinder pressure measured by the in-cylinder pressure during the intake stroke was imposed equal to the average pressure measured by an absolute pressure sensor (Kistler piezoresistive sensor type 4045A2) mounted along the intake duct. Then, the absolute cylinder pressure so obtained was stored for 50 consecutive cycles, averaged and then post-processed. The gross HRR was calculated as:

$$\mathrm{HRR} = \frac{dQ_{\mathrm{net}}}{d(\mathrm{CAD})} + \frac{dQ_w}{d(\mathrm{CAD})} \tag{10.1}$$

The term $\frac{dQ_{\mathrm{net}}}{d(\mathrm{CAD})}$ was estimated based on the single-zone simplified model:

$$\frac{dQ_{\mathrm{net}}}{d(\mathrm{CAD})} = \frac{k}{k-1} p_{\mathrm{cyl,abs}}(\mathrm{CAD}) \frac{dV(\mathrm{CAD})}{d(\mathrm{CAD})} + \frac{1}{k-1} V(\mathrm{CAD}) \frac{dp_{\mathrm{cyl,abs}}(\mathrm{CAD})}{d(\mathrm{CAD})} \tag{10.2}$$

where k is the heat capacity ratio (assumed equal to 1.38) and V(CAD) is the cylinder volume variable with CAD. The term $\frac{dQ_w}{d(\mathrm{CAD})}$, accounting for the heat transfer through the cylinder walls, has been estimated as:

$$\frac{dQ_w}{d(\mathrm{CAD})} = A_{ht} h_c (T - T_w) \tag{10.3}$$

where A_{ht} is the instantaneous cylinder heat exchange surface (crown of a cylinder head, cylinder walls, and piston head), T is the instantaneous cylinder average temperature, T_w is the average temperature of the inner cylinder surface, while the total heat transfer coefficient h_c was estimated as proposed by Woschni (1967). The estimated error in this calculation, due to the errors in the absolute cylinder pressure measurement, is around 2%. Based on $p_{\text{cyl,abs}}$, it was possible to estimate the indicated power P_i supplied by the engine:

$$P_i = \frac{n}{n_R} \oint_{\text{cycle}} p_{\text{cyl,abs}} dV \tag{10.4}$$

where n is the engine speed, while n_R (=2 in this case) is the number of crank revolutions for each power stroke. The average diesel fuel consumption was measured by means of an AVL 733S fuel balance. The methane flux was stabilized by means of a 0.8 L plenum positioned upstream the methane injector. The average methane fuel consumption G_{gas} was measured by means of a thermal mass flow, Aalborg Instruments and Controls Inc., model DFC 36 characterized by a measurement error below 1%. The measurement of the fuel consumption allowed to estimate the fuel conversion efficiency referred to the indicated power, η_f:

$$\eta_f = \frac{P_i}{\dot{m}_d H_{i,d} + G_{\text{gas}} H_{i,\text{gas}}} \tag{10.5}$$

where $H_{i,d}$ and $H_{i,\text{gas}}$ are the lower calorific values, respectively, of diesel fuel and methane. The combustion efficiency was calculated as:

$$\eta_b = 1 - \frac{\sum x_i H_{i,i}}{\left(\frac{\dot{m}_d H_{i,d} + G_{\text{gas}} H_{i,\text{gas}}}{\dot{m}_a + \dot{m}_d + G_{\text{gas}}} \right)} \tag{10.6}$$

in which x_i is the mass fractions of CO and THC measured at the exhaust, $H_{i,i}$ the related lower calorific values, and $\dot{m}_a$ is the consumed intake air mass measured by means of an AVL FLOWSONIX mounted between two plenums in order to stabilize the air flux. Because the composition of THC in the exhaust, and thus the related $H_{i,i}$, is not known, the combined mass-fraction-weighted H_i of diesel fuel and methane has been used to represent the lower calorific value of THC.

The efficiency of the thermodynamic cycle was calculated as:

$$\eta_c = \frac{\eta_f}{\eta_b} \tag{7}$$

The combustion products and therefore the pollutant emission levels at the engine exhaust have been measured by means of an AVL AMA i60 Exhaust Measurement System.

In particular, THC levels have been measured through AVL flame ionization detector (FID) analyzer, whose operation is based on the measurement of the electrical current yield by the organic carbon atoms ionized in a hydrogen flame. NO_x levels were measured through AVL chemiluminescence detector (CLD) analyzer, whose operation is based on the measurement of the light emitted during the oxidation of nitrogen oxide NO with ozone O_3, and CO levels have been measured through an infrared detector (IRD) analyzer, whose operation is based on the measurement of an infrared radiation absorption, correlated to the concentration of the component to be measured. Particulate matter at tailpipe was not measured since, as observed in several engine working conditions, the emission levels were always well below 1 mg/m^3.

10.3 Results and Discussion

10.3.1 Effect of SOI Spanning on Combustion Development

Figure 10.2 shows the HRR histories calculated on the basis of cylinder pressure measured at n = 1500 rpm for different pilot timings (varied from −50 CAD ATDC up to 10 CAD ATDC). Injection and engine settings were: CR = 17; p_rail = 1250 bar; ICP = 1.16 bar. Tests have been run injecting always the same amount of pilot diesel fuel ($(\dot{m}_d = 6\,\mathrm{mm}^3/\mathrm{cycle})$), while varying the amount of introduced methane: In detail, plot shows data (a) with no methane (OD); (b) with low/medium methane amount (LM); and (c) with medium/high methane amount (MH). The combustion development observed for all the injection and engine settings can be summarized in the following macrotrends:

- Advanced SOI and low amounts of methane (plot a) show a gradually weaker HRR, characterized by a first heat release at very advanced CAD (around −20 CAD ATDC, likely associated with LTC) followed by a second heat release phase; as the methane is increased (plots b and c), this second heat release phase shows an increasing peak.
- Retarding SOI (plot a) leads to a HRR shape closer to the one observed with the conventional diesel combustion: a premixed peak followed by a queue characterized by a lower HRR. In this case too, this second combustion phase is more pronounced as the methane introduced in the cylinder is increased (plots b and c).

In Fig. 10.3, the above observations are summarized. In particular, referring to Fig. 10.3a, for low/medium values of methane rates, HRR peak first increases as SOI is retarded from very advanced SOI and then decreases as SOI is further retarded after TDC. This trend is still observed as the methane rate is increased; however, the SOI related to the maximum HRR is gradually advanced and

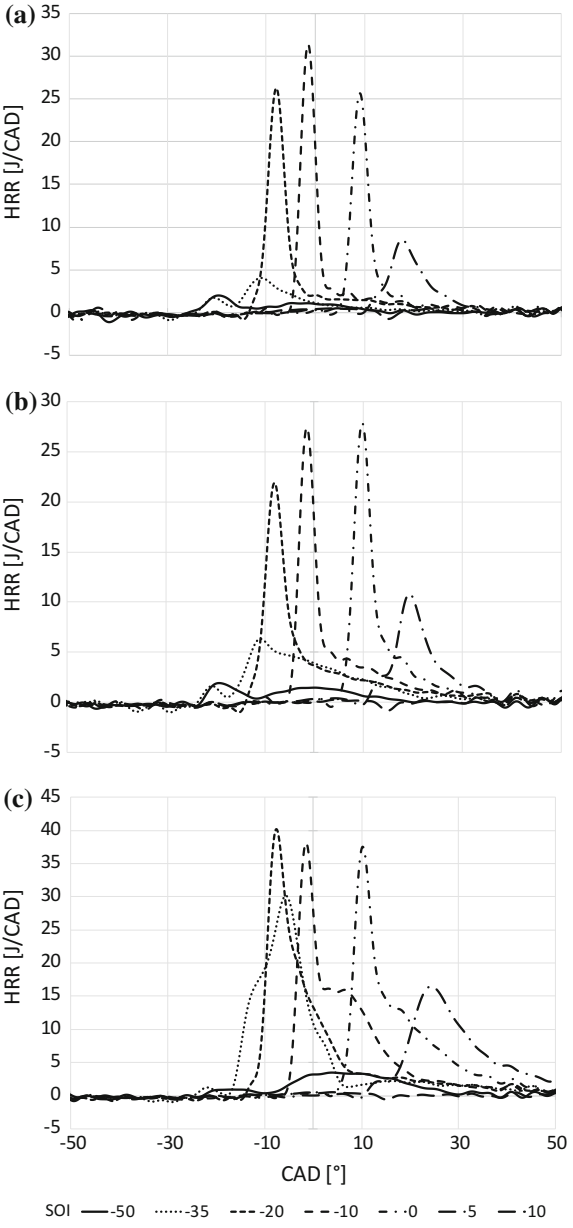

Fig. 10.2 HRR versus CAD for variable methane rate: **a** OD; **b** L; **c** M. CR = 17; p_rail = 1250 bar; ICP = 1.16 bar

maximum values globally increase. The CAD corresponding to maximum HRR is first advanced as SOI is retarded from very advanced SOI and then is delayed. Methane rate has a secondary influence on CAD corresponding to maximum HRR. This behavior, already described in the literature, is mainly due to the behavior of

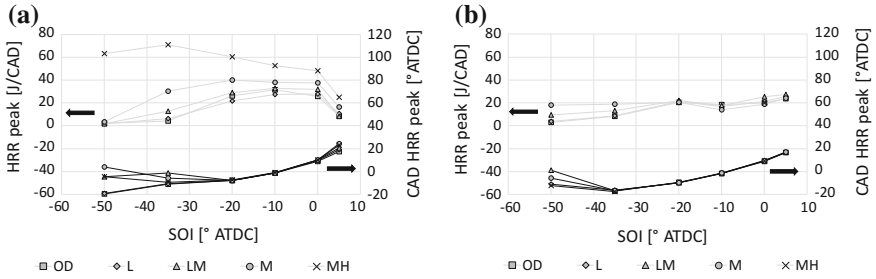

Fig. 10.3 HRR peak and related CAD as a function of SOI for different methane rates. **a** CR = 17, p_rail = 1250 bar, ICP = 1.16 bar; **b** CR = 17, p_rail = 500 bar, ICP = 1.66 bar

the ignition delay combined with the equivalence ratio distribution inside the combustion chamber. As SOI is advanced, ignition delay is prolonged which can lead to overlearning of the mixture and low combustion rate. On the other hand, as SOI is retarded, ignition conditions may not be reached due to temperature reduction during the expansion phase. The combustion development just described was observed for all combinations of CR, p_rail, and ICP tested during the present experimental campaign with the exception of CR = 17, ICP = 1.66, p_rail = 500/1250 bar, for which the observed behavior is reported in Fig. 10.3b. The main differences that can be noted with previous plots are: for retarded SOI, the HRR peak exhibits an increasing trend; in these conditions, the effect of increasing methane is not univocally defined.

In the following, the combustion development has been characterized in terms of: ignition delay, ID, defined as the angular difference between the SOI and the angle at which 5% of the total heat has been released; maximum pressure rise rate, MPRR; combustion beginning, CA5, defined as the angle at which 5% of the total heat has been released; center of combustion, CA50, defined as the angle at which 50% of the total heat has been released; and combustion duration, CA90-CA10, defined as the angular difference between the angles at which 90 and 10% of the total heat has been released. Then, the effects of ICP, CR, and p_rail on the above parameters have been analyzed. It shall be emphasized that the injection event was always decoupled from the start of combustion, due to the short duration of pilot injection. Therefore, the behavior of the difference between the start of combustion and the end of injection follows the same trend of ID assuming values always higher than zero.

10.3.2 Effect of Intake Charge Pressure

In Fig. 10.4, the effect of ICP (ICP = 1.16 bar, column "a"; ICP = 1.66 bar, column "b") at different SOI and for different methane rates on ID and MPRR, plots (a′) and (b′); CA5, CA50, and CA90-CA10, plots (a″) and (b″), is highlighted. The engine

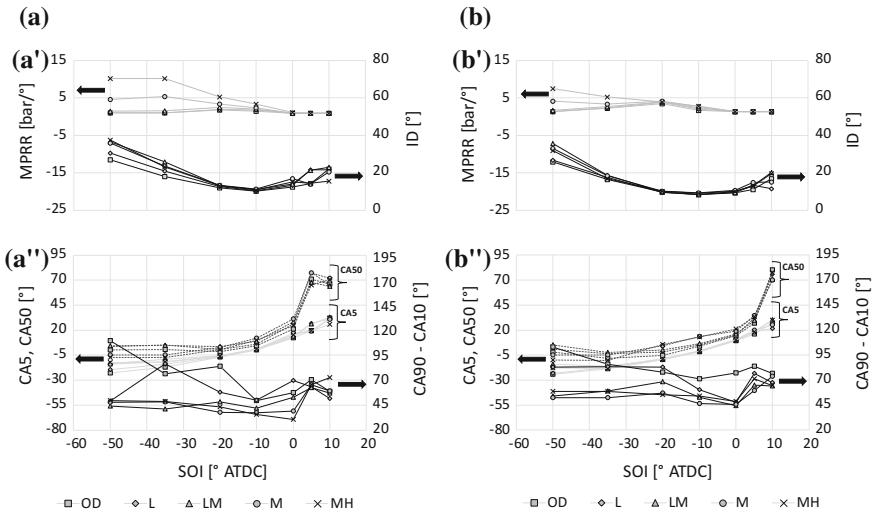

Fig. 10.4 Effect of intake charge pressure (ICP = 1.16 bar, column "a"; ICP = 1.66 bar, column "b") at different SOI and for different methane rates on: ID and MPRR, plots (**a**′) and (**b**′); CA5, CA50, and CA90-CA10, plots (**a**″) and (**b**″). CR = 14; p_rail = 500 bar

volumetric compression ratio was fixed equal to 14 and the injection pressure to 500 bar.

Concerning ID (plots a′ and b′), a decreasing–increasing behavior is visible with SOI spanning. In particular, ID reaches the highest values—about 40 CAD—with the highest SOI advances, due to the low temperature at which the injection is performed. In these conditions, the limiting factor is represented by the preignition reaction rates (slower at a lower temperature), as there is sufficient time for diesel evaporation and effective mixing with the surrounding methane–air mixture. As SOI is retarded, ID decreases up to a certain value (around 10 CAD), as the temperature in the cylinder during injection is higher; then, it increases again, because the cylinder temperature during injection decreases again. This behavior has been broadly documented in the literature [see, for example, Guerry et al. (2016)] and was observed for all the other investigated combinations of engine volumetric compression ratio and pilot injection pressure. It must be specified, however, that, for the two combinations of Fig. 10.3b, the increasing trend when retarding SOI was much less pronounced.

It is visible that the methane rate has a secondary effect on ID compared to SOI. Only-pilot diesel injection condition, however, exhibits, as expected, the lowest values of ID. This behavior too has been broadly documented in the literature; see, for example, Hosmath et al. (2016).

Comparing curves varying ICP (plots a′ and b′), it can be noted that also this parameter has a secondary effect on ID. In any case, the observed trend, i.e., a reduction of ignition delay as ICP is increased, especially for central values of SOI

in the tested interval, has been already described, for example, in Guerry et al. (2016). The above conclusions that can be extended to all the other investigated combinations of engine compression ratio and injection pressure mainly occur because the in-cylinder pressure both before and during combustion is higher increasing ICP; consequently, ignition occurs earlier. Another related aspect of the ICP variation is that the overall equivalence ratio is also allowed to vary with ICP. Clearly, the temporal phasing of the HRR curves is also affected by the overall equivalence ratios.

Concerning MPRR (plots a′ and b′), a strong variability is evident with SOI. At low/medium methane rate, MPRR associated with very advanced SOI is very low, then increases to higher values at intermediate SOI, and then decreases again up to very low values with retarded SOI. SOI values determining a very low MPRR are associated with a very slow combustion development, as already described in the previous section. This behavior has been documented, for example, in Raihan et al. (2015). As the amount of methane introduced in the cylinder is increased, MPRR behavior varies significantly. Values associated with very advanced SOI are very high; however, the trend becomes strictly decreasing [as shown in Guerry et al. (2016) for tests conducted at high BMEP] and MPRR values gradually reach those observed at low/medium methane rate as SOI is retarded. The effect of ICP (compare plots a′ and b′), observed for all combinations of engine compression ratio and injection pressure, is to reduce significantly the absolute value of MPRR at medium/high methane rates, while there is a slight increase at low/medium methane rate. This trend is possibly due to a more limited atomization and vaporization of pilot fuel droplets acting as ignition agents for the premixed methane/air phase.

Concerning CA5 angles (plots a″ and b″), it is visible that it is advanced as SOI is advanced. For the most advanced SOI, it is visible, however, that CA5 reaches a plateau and, for several combinations of engine compression ratio and injection pressure, it actually starts increasing. This trend too has been documented in the literature [see, for example, Guerry et al. (2016)].

CA50 (plots a″ and b″) follows a similar behavior as far as SOI is between the most advanced and intermediate values. For retarded SOI, however, the difference between CA50 and CA5 increases evidently, which denotes a slower combustion development attributable to the lower pressure and temperature into the cylinder associated with very delayed SOI.

Concerning CA90-CA10 (plots a″ and b″), a trend first decreasing, then increasing, and then decreasing again when retarding SOI was observed for most of methane flow rates. This trend, observed for all combinations of engine compression ratio and injection pressure, is not in agreement with what observed, for example, in Guerry et al. (2016). It is worth noting, moreover, that the difference between CA50 and CA5, previously underlined for retarded SOI, does not excessively penalize combustion overall duration. It is also evident that the effect of methane rate is secondary and appears more evident at low/medium rates. Increasing methane amount, however, determines a reduction in combustion duration, which will lead—as analyzed in the following—to a corresponding increase in fuel conversion efficiency.

Increasing ICP very slightly decreases CA5; CA50 starts differentiation from CA5 with SOI equal to 5 at low ICP, while at high around 10. This leads to the conclusion that higher ICP sustains the combustion with more retarded SOI. Finally, combustion duration (CA90-CA10) is slightly higher at higher ICP. Again, this trend is confirmed for all combinations of engine compression ratio and injection pressure.

In Fig. 10.5, the effect of intake charge pressure (ICP = 1.16 bar, column "a"; ICP = 1.66 bar, column "b") at different SOI and for different methane rates on η_b and η_f, plots (a′) and (b′); CO and THC, plots (a″) and (b″); and NO_x, plots (a‴) and (b‴), is highlighted (note that the interval of SOI has been limited to −50–0 ATDC given that, for more retarded SOI, the engine η_f is equal to zero and the results do not have practical sense). As for plots in Fig. 10.4, the engine volumetric compression ratio was equal to 14 and the injection pressure to 500 bar.

The behavior of η_b is reported in Fig. 10.5, plots a′ (low ICP) and b′ (high ICP). As visible, at low/medium methane rate, the behavior is increasing and then decreasing when SOI is retarded. This trend is due to the fact that, as already analyzed through HRR curves, at very advanced or retarded SOI, combustion is very poor (see Fig. 10.2a); therefore, a large amount of fuel is discharged along the exhaust line, as will be evident analyzing THC and CO emission levels in these

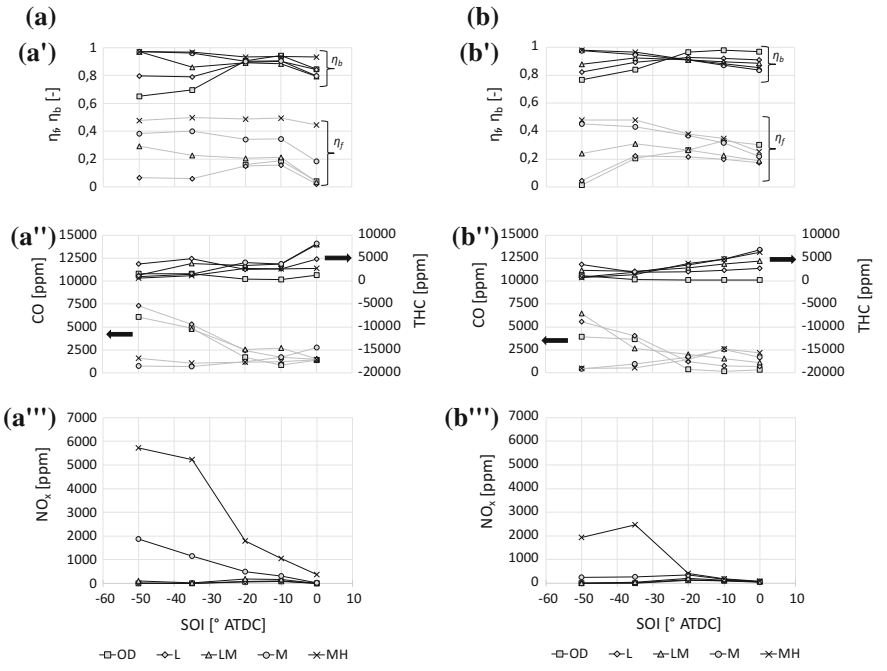

Fig. 10.5 Effect of intake charge pressure (ICP = 1.16 bar, column "a"; ICP = 1.66 bar, column "b") at different SOI and for different methane rates on: η_b and η_f, plots (**a**′) and (**b**′); CO and THC emission levels, plots (**a**″) and (**b**″); NO_x emission levels, plots (**a**‴) and (**b**‴). CR = 14; p_rail = 500 bar

conditions. Increasing methane rate, combustion is poor only at very retarded SOI (see Fig. 10.2c): in these conditions again, a large amount of fuel is exhausted, so determining a significant reduction of η_b. At very advanced SOI, on the other hand, η_b is close to unity. η_b is basically unaffected by ICP being its effect evident only at low methane rate and very advanced SOI. Concerning η_c, the effect of methane rate is to increase η_c. The fuel conversion efficiency η_f is therefore strictly increasing at medium/high methane rates [in agreement with results reported in Guerry et al. (2016)], while it is increasing and then decreasing at low methane rates as SOI is advanced (plots a′ and b′). An increase of ICP negatively affected η_f at medium/high methane rates and central SOI.

THC levels increase as SOI is retarded; moreover, from low to medium methane rates, THC increases, while from medium to medium/high methane rates THC decreases. If indicated specific emission levels were considered instead of [ppm], the trend would have been increasing as methane rate decreases. These trends are in agreement with results reported in Guerry et al. (2016). On the other hand, CO emission levels ehibit a more complicated behavior. They decrease as SOI is retarded at low/medium methane rate, while they show an increasing/decreasing behavior at medium/high rates. In this case too, if indicated specific emission levels were considered instead of [ppm], the trend would have been increasing as methane rate decreases.

It is widely recognized that THC emissions are determined by many causes: valve overlap, flame quenching, wall impingement, spray characteristics, crevices, in-cylinder conditions, and residence time. CO emissions, on the other hand, are mainly due to flame quenching, crevices, residence time, in-cylinder conditions. In a dual-fuel HCCI engine—with methane fumigated along the intake duct—the major sources are valve overlap, crevices, and bulk quenching of the diesel–methane–air mixture, with the in-cylinder bulk temperature having a significant influence on THC and CO oxidation rates, with the former faster than the latter.

In Fig. 10.6, the maximum in-cylinder bulk temperature is reported, at different SOI and for different methane rates (ICP = 1.16 bar, plot “a”; ICP = 1.66 bar, plot “b”).

From plot “a”, it can be observed that maximum in-cylinder bulk temperature is not sensitive to SOI for low methane rates, while it decreases as SOI is retarded at medium/high methane rates. This is consistent with the THC levels observed in Fig. 10.5 plot b″. On the other hand, from low to medium methane rates, THC increase as well as maximum in-cylinder bulk temperature, it could be argued because of crevice hydrocarbons not being oxidized because of the excessively lean methane–diesel–air mixture together to mixture escaping during valves overlap. Increasing methane rate from medium to high values, however, the mixture is not further excessively lean and crevice hydrocarbons can be—at least partially—oxidized. It is believed that no wall impingement by spray liquid phase takes place, based on data reported in Carlucci et al. (2014, 2015, 2017).

Concerning CO, a marginal increase is observed at retarded SOI, while THC increase is sharper; at very advanced SOI, CO increase is sharper than THC increase, according to results published in Guerry et al. (2016).

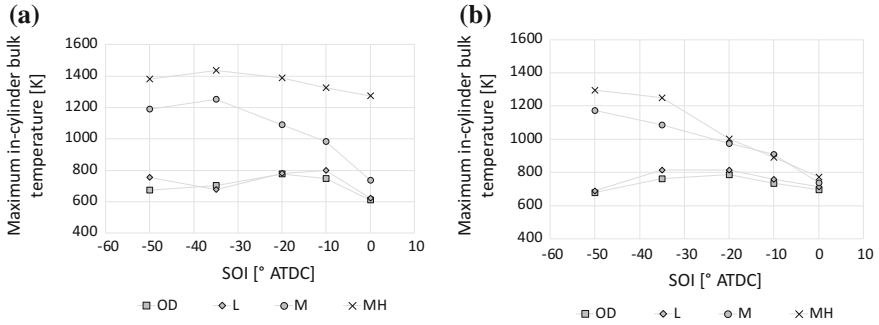

Fig. 10.6 Effect of intake charge pressure (ICP = 1.16 bar, plot "a"; ICP = 1.66 bar, plot "b") at different SOI and for different methane rates on maximum in-cylinder bulk temperature. CR = 14; p_rail = 500 bar

Increasing ICP has a direct and an indirect effect on many of the abovementioned causes determining THC and CO emission levels: In particular, more oxygen is available for oxidation, but at the same time the mixture equivalence ratio decreases; more fresh methane–air mixture escapes during valve overlap; due to the different in-cylinder pressure and temperature histories, both the residence time and the diesel spray properties vary. The effect of ICP on each of these causes is hard to be quantified; the overall observed effect is that, increasing ICP, THC is reduced. On the other hand, CO emission levels decrease as ICP increases.

NO_x emission levels are shown in Fig. 10.5 plot a‴. In particular, at low/medium methane rate, NO_x emissions increase and then decrease as SOI is retarded, in agreement with results reported in Guerry et al. (2016). At medium/high methane rate, the behavior is strictly decreasing as SOI is retarded. NO_x emission behavior as a function of SOI and methane reproduces the behavior of maximum bulk temperature in Fig. 10.6 being dependent, as modeled by Zeldovich mechanism, on local temperature, residence time, and oxygen availability. The effect of ICP is to significantly reduce NO_x emissions.

10.3.3 Effect of Engine Volumetric Compression Ratio

In Fig. 10.7, the effect of engine volumetric compression ratio (CR = 14, column "a"; CR = 17, column "b") at different SOI and for different methane rates on ID and MPRR, plots (a′) and (b′); CA5, CA50, and CA90-CA10, plots (a″) and (b″), is highlighted. The injection pressure and the ICP were, respectively, set equal to 500 bar and 1.16 bar.

Comparing both ID, it is visible that the effect of compression ratio increase is to reduce both of them, for all combinations of ICP and injection pressure. Indeed, thanks to the higher in-cylinder pressure reached during compression phase,

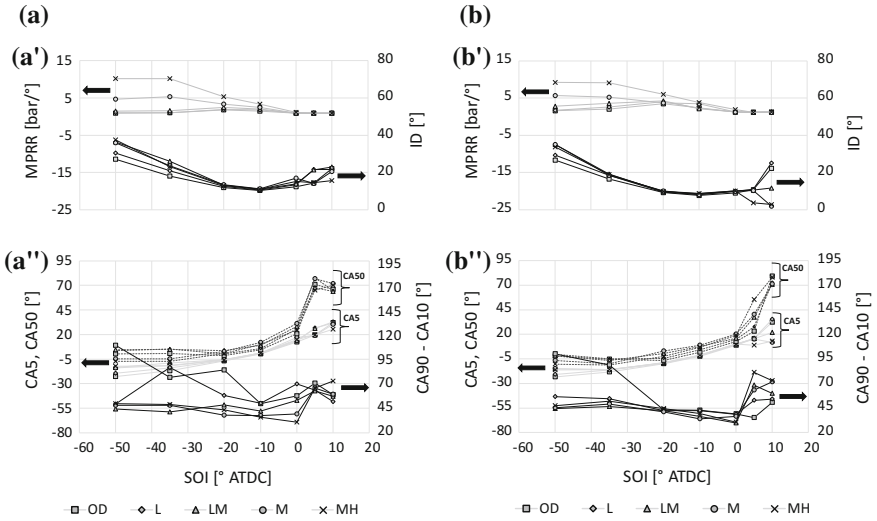

Fig. 10.7 Effect of engine volumetric compression ratio (CR = 14, column "a"; CR = 17 bar, column "b") at different SOI and for different methane rates on: ID and MPRR, plots (**a**′) and (**b**′); CA5, CA50, and CA90-CA10, plots (**a**″) and (**b**″). p_rail = 500 bar; ICP = 1.16 bar

preignition reactions are accelerated and ID reduced. However, as already seen discussing the effect of ICP, ID shortening reduces the premixed combustion intensity. The result is that MPRR does not vary significantly with CR.

Increasing engine compression ratio, CA90-CA10 is reduced at low/medium methane rates, while at higher rates the values are comparable. CA5 and CA50 are similar up to SOI = 0 at low compression ratio, while at high compression ratio the two angles remain similar up to SOI = 5 ATDC. The observed trends are in good agreement with those presented in Hosmath et al. (2016). This leads to the conclusion that a higher CR sustains the combustion with more retarded SOI.

In Fig. 10.8, the effect of engine volumetric compression ratio (CR = 14, column "a"; CR = 17, column "b") at different SOI and for different methane rates on η_b and η_f, plots (a′) and (b′); CO and THC, plots (a″) and (b″); and NO_x, plots (a‴) and (b‴), is highlighted.

The effect of increased compression ratio is to increase η_b at low/medium methane rates, as visible comparing plots a′ (low compression ratio) and b′ (high compression ratio) of Fig. 10.8 for all combinations of ICP and p_rail. The effect of compression ratio is to extend the SOI range for which fuel conversion efficiency η_f is high, this especially at low/medium methane rates, while at high rates the values are not sensibly affected by compression ratio, this result being confirmed by results reported in Di Blasio et al. (2017a).

THC is slightly reduced by variation of compression ratio, while CO is reduced at low/medium methane rate, especially at central values of SOI, in good agreement with results reported in Di Blasio et al. (2017a). As already discussed in

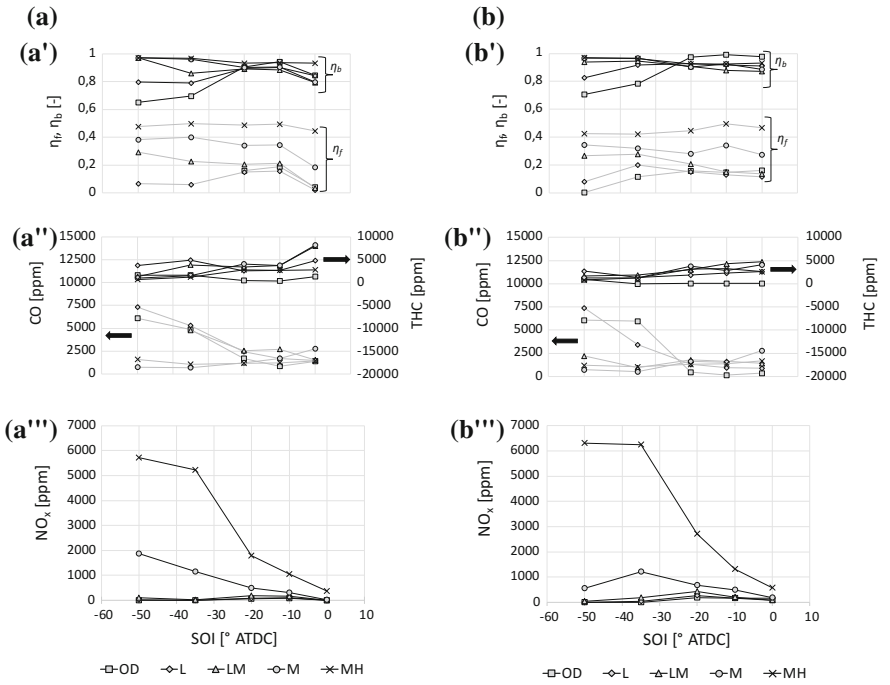

Fig. 10.8 Effect of engine volumetric compression ratio (CR = 14, column "a"; CR = 17, column "b") at different SOI and for different methane rates on: η_b and η_f, plots (**a**′) and (**b**′); CO and THC emission levels, plots (**a**″) and (**b**″); NO_x emission levels, plots (**a**‴) and (**b**‴). p_rail = 500 bar; ICP = 1.16 bar

Sect. 10.3.2, the causes determining THC and CO are many and complex to be quantified. Among them, CR has an effect on spray properties, in-cylinder pressure and temperature histories and residence time. NO_x is increased as compression ratio is increased, due to higher in-cylinder temperature (not shown) and longer residence time.

10.3.4 Effect of Injection Pressure

In Fig. 10.9, the effect of pilot injection pressure (p_rail = 500 bar, column "a"; p_rail = 1250 bar, column "b") at different SOI and for different methane rates on ID and MPRR, plots (a′) and (b′), and CA5, CA50, and CA90-CA10, plots (a″) and (b″), is highlighted. The engine compression ratio was equal to 17, while the intake pressure was set equal to 1 bar.

Comparing ID, it is visible that the effect of injection pressure increase is to increase ID when SOI is advanced, for all combinations of ICP and engine compression ratio. The variable effect of p_rail with SOI is mainly due to the fact that, at

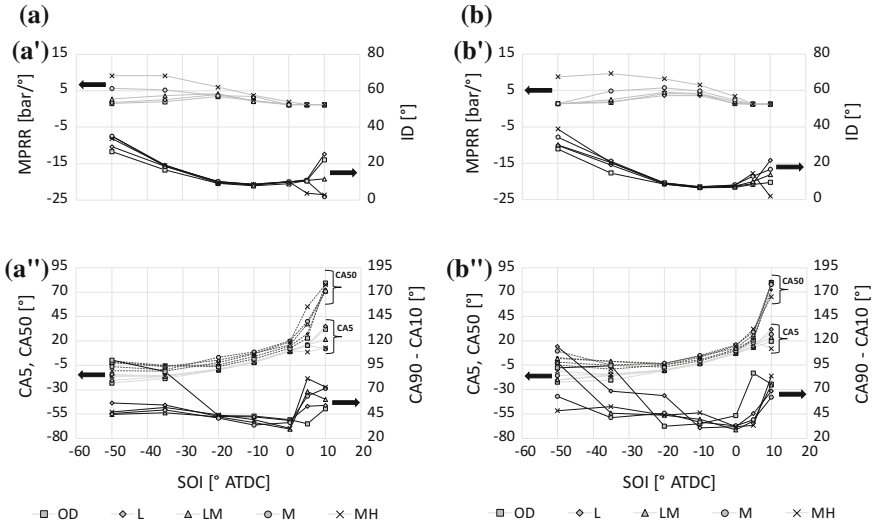

Fig. 10.9 Effect of injection pressure (p_rail = 500 bar, column "a"; p_rail = 1250 bar, column "b") at different SOI and for different methane rates on: ID and MPRR, plots (**a**′) and (**b**′); CA5, CA50 and CA90-CA10, plots (**a**″) and (**b**″). CR = 17; ICP = 1.16 bar

very advanced or retarded SOI, chemical ID dominates on physical ID, while the contrary happens for central values of SOI (Carlucci et al. 2017). Concerning MPRR, the effect of injection pressure is always to slightly increase MPRR. All these trends are confirmed by data reported in Raihan et al. (2015).

CA90-CA10 is slightly reduced. CA5 and CA50 are similar up to SOI = 0 at a low injection pressure, while at high injection pressure the two angles remain similar up to SOI = 5 ATDC. Again, this suggests that with higher p_rail the combustion can be sustained for more retarded SOI.

In Fig. 10.10, the effect of p_rail (p_rail = 500 bar, column "a"; p_rail = 1250 bar, column "b") at different SOI and for different methane rates on η_b and η_f, plots (a′) and (b′); CO and THC, plots (a″) and (b″); and NO_x, plots (a‴) and (b‴), is highlighted.

A not very evident effect of injection pressure increase is observed on η_b, while η_f is increased specially at low/medium methane rates, this trend confirmed by data reported in Raihan et al. (2015). At medium/high methane rate, the values are affected by injection pressure only at very advanced SOI, where a reduction is observed when injection pressure is increased.

CO and THC emissions in ppm are reported in Fig. 10.10 plots a″ and b″. The effect of injection pressure on THC is a slight reduction, especially at low methane rates, as injection pressure is increased, in agreement with results reported in Raihan et al. (2015). An opposite behavior is observed only for advanced SOI. On the other hand, CO is increased, in agreement with results reported in Raihan et al. (2015). As already discussed in Sect. 10.3.2, the causes determining THC and CO are many

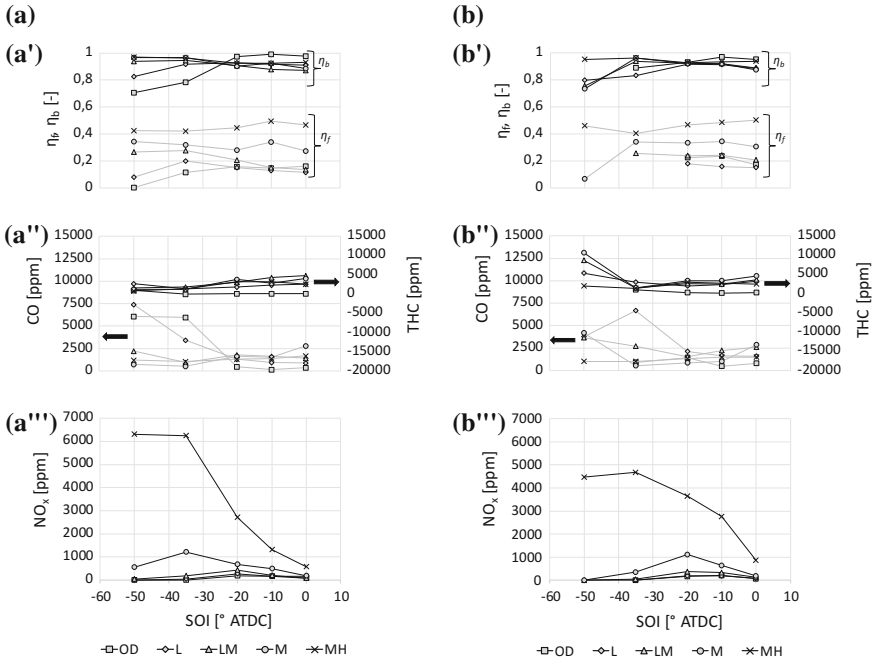

Fig. 10.10 Effect of injection pressure (p_rail = 500 bar, column "a"; p_rail = 1250 bar, column "b") at different SOI and for different methane rates on: η_b and η_f, plots (**a**′) and (**b**′); CO and THC emission levels, plots (**a**″) and (**b**″); NO_x emission levels, plots (**a**‴) and (**b**‴). CR = 17; ICP = 1.16 bar

and complex to be quantified. Among them, p_rail has an effect mainly on spray properties and indirectly on in-cylinder pressure and temperature histories and residence time.

Finally, NO_x levels are reported in Fig. 10.10 plots a‴ and b‴. The effect of p_rail increase is to decrease NO_x levels. This result, in agreement with similar data reported in Raihan et al. (2015), can be attributed to the fact that, given the little amount of diesel pilot fuel, higher injection pressures lead to faster vaporization and better fuel–air mixing which in turn facilitates better mixing of high-temperature diesel combustion zones with leaner, low-temperature methane combustion zones. Overall, this leads to a reduction in NO_x at the engine exhaust.

10.3.5 Factor Settings Approaching HCCI Operation

As already said, the total amount of tests is very high and it is not convenient, for the sake of brevity, to report all the results. However, it is important to investigate the factor variation ranges leading the engine to operate in or close to HCCI

combustion, i.e., guaranteeing a high conversion efficiency and low emission levels at the same time.

In Table 10.3, the range of SOI able to guarantee a NO_x level lower than 2 g/kWh and η_f and THC values comparable with those measured for "conventional" SOI are highlighted for each combination of engine compression ratio, injection pressure, and ICP. Moreover, a cell colored in light gray, dark gray, or black means that the above result was obtained, respectively, at low, low/medium, or medium/high methane rate.

From Table 10.3, it is possible to recognize that:

- A significant reduction of NO_x levels, keeping high values of η_f and THC, can be obtained with very advanced pilot injections; in these conditions, however, the benefit is limited to low/medium methane rates. In order to reach these conditions, it is preferable to have lower values of engine compression ratios; the utilization of a high compression ratio was effective only with a proper choice of injection pressure and ICP.
- A significant reduction of NO_x levels, keeping high values of η_f and THC, can be also obtained retarding SOI after TDC. In these conditions, it is visible that the benefits are not limited only to low/medium methane rates, but are extended also at high rates. In order to reach these conditions, a high value of ICP is preferable, although good results were also reached with low intake pressure combined with a high injection pressure and a high engine compression ratio.

Table 10.3 Factor settings guaranteeing NO_x level lower than 2 g/kWh and η_f and THC values comparable with those measured for "conventional" SOI

SOI [CADATDC]	−50	−35	−20	−10	0	5
14/500/1.16						
14/1250/1.16						
17/500/1.16						
17/1250/1.16						
14/500/1.66						
14/1250/1.66						
17/500/1.66						
17/1250/1.66						

Therefore, in order to obtain a homogeneous mixture and consequently a lean combustion, the longer ID obtained with very advanced or very retarded injections can be exploited. The first approach has been abundantly studied and documented in the open literature, some of which is cited in the present chapter. The second approach, on the other hand, did not receive attention so far. However, in diesel HCCI, a combustion concept exploiting very retarded injections has been already proposed, highlighting three main advantages: first, late injections are applicable with conventional technology already available for diesel engines; second, injection and combustion processes are not completely decoupled, so that combustion phasing is controlled by injection timing; third, very advanced injections determine impingement on the walls, which also shorten the average life of the lubricating oil by an excessive dilution of the fuel that wets the walls during the compression phase. This concept is the basis of the modulated kinetics (MK) combustion.

In the first generation of the MK system, success of combustion with HCCI characteristics relied on three factors. First, oxygen concentration and local temperature in the cylinder were reduced with EGR, so determining a drastic reduction in NO_x emission but also an increase in soot and THC. Second, as previously said, the fuel injection was retarded, and so the ID prolonged, which led to a more premixed combustion with lower NO_x, lower soot, but higher THC emission mainly due to wall impingement. Third, a high swirl ratio was used in order to improve the mixture formation, further reducing soot emission and avoiding wall impingement, so leading to a drastic reduction in THC (Kimura et al. 1997).

In the second generation of the MK combustion system, studied in order to broaden the load and speed range of application, the autoignition delay was increased reducing the compression ratio and cooling the EGR. Moreover, the injection duration was reduced increasing the injection pressure (Kimura et al. 2001).

It could be argued that generally, by delaying the injection, the thermal efficiency is lowered. In MK combustion, this disadvantage is compensated by the high swirl and, therefore, by the low production of THC, which brings the thermal efficiency to levels comparable or even higher than diesel conventional combustion. MK combustion, moreover, is slower in the initial phase than the conventional one—thus, a reduction of the combustion noise is obtained—however, it grows vigorously during the second part of the combustion. This means that the combustion duration for the two cases is comparable.

In DF combustion concept, however, late injection potential addressed to establish HCCI combustion has not been investigated. In Fig. 10.11, in-cylinder pressure, HRR, HRR cumulative, and in-cylinder bulk temperature curves are reported, related to two "limit" cases: in 14-500-1.16 tests with SOI at TDC, an η_f value close to zero was measured at low/medium methane rates, while at medium/high rates it was significantly lower than that measured at more advanced SOI (Fig. 10.5 plot a′). THC was lower as well as CO at low and medium/high methane rates (at medium rates, they slightly increased compared to more advanced SOI; see Fig. 10.5 plot a″). NO_x was almost zero (Fig. 10.5 plot a‴). In 17-1250-1.16 tests, on the other hand, η_f assumes values comparable to those assumed at more

advanced SOI for all methane rates, with no penalty on THC, a very little penalty at medium/high methane rates in terms of CO and low NO_x specially at low/medium rates (see Fig. 10.10, column b). Still in Fig. 10.11, the effect of the increase of methane rate is highlighted. When compression ratio, injection pressure, and intake pressure are low (plot a″), the HRR associated with diesel combustion exhibits very low HRR values; therefore, the combustion duration is several tens of CAD. This is due to lower in-cylinder local temperatures deriving from both lower CR and ICP associated with the low injection pressure leading to poor atomization and slower vaporization. The addition of methane further penalizes the pilot combustion, as the HRR further decreases in the initial stage of combustion; as a consequence, methane combustion is slow as well and can be considered complete around 60 CAD ATDC.

As CR and injection pressure are increased (plot b″), the behavior is totally different. The HRR rate associated with the diesel fuel is much higher, so the combustion duration is strongly decreased. Moreover, the addition of methane does not affect negatively the pilot combustion. On the contrary, HRR increases, which is due to the combustion of methane. The remaining part burns more slowly during the queue, but the combustion can be considered complete well before the previous case. In fact, analyzing the cumulative HRR (plots a‴ and b‴) highlights that, in the first case, the total heat released remains low; the presence of methane further reduces it. In the second case, on the contrary, the total heat released is significantly higher and further increases if methane is added. The analysis of in-cylinder bulk temperature, reported in plots a⁗ and b⁗, further confirms a more complete combustion with high values of compression ratio and injection pressure. The high-temperature values reached during the expansion stroke help the oxidation of THC and CO species without penalizing NO_x emission.

Therefore, the elements characterizing MK can be seen also in DF combustion. This, therefore, shall stimulate the study of the effect of EGR (hot and cooled) and swirl, combined with variable injection pressure and engine compression ratio, as improvers of MK combustion, whose beneficial effect has been already proved for diesel HCCI combustion.

10.4 Factorial Analysis

In Sect. 10.2, Table 10.2, it has been highlighted that each factor varies on a certain number of levels; being 5 the variation levels of the methane rate, 7 the variation levels of pilot injection timing and 2 the variation levels of the injection pressure, engine volumetric compression ratio, and ICP, the complete factorial plan made of 5 * 2 * 7 * 2 * 2 = 280 possible combinations was therefore performed. In this section, the results of the factorial analysis will be described, conducted on: IMEP, η_f, MPRR, THC, CO, and NO_x. Therefore, the influence of each factor (first-order effects) as well as of combinations of factors (second-order effects), on the output parameters, has been quantified. To achieve this goal, the ANOVA technique was

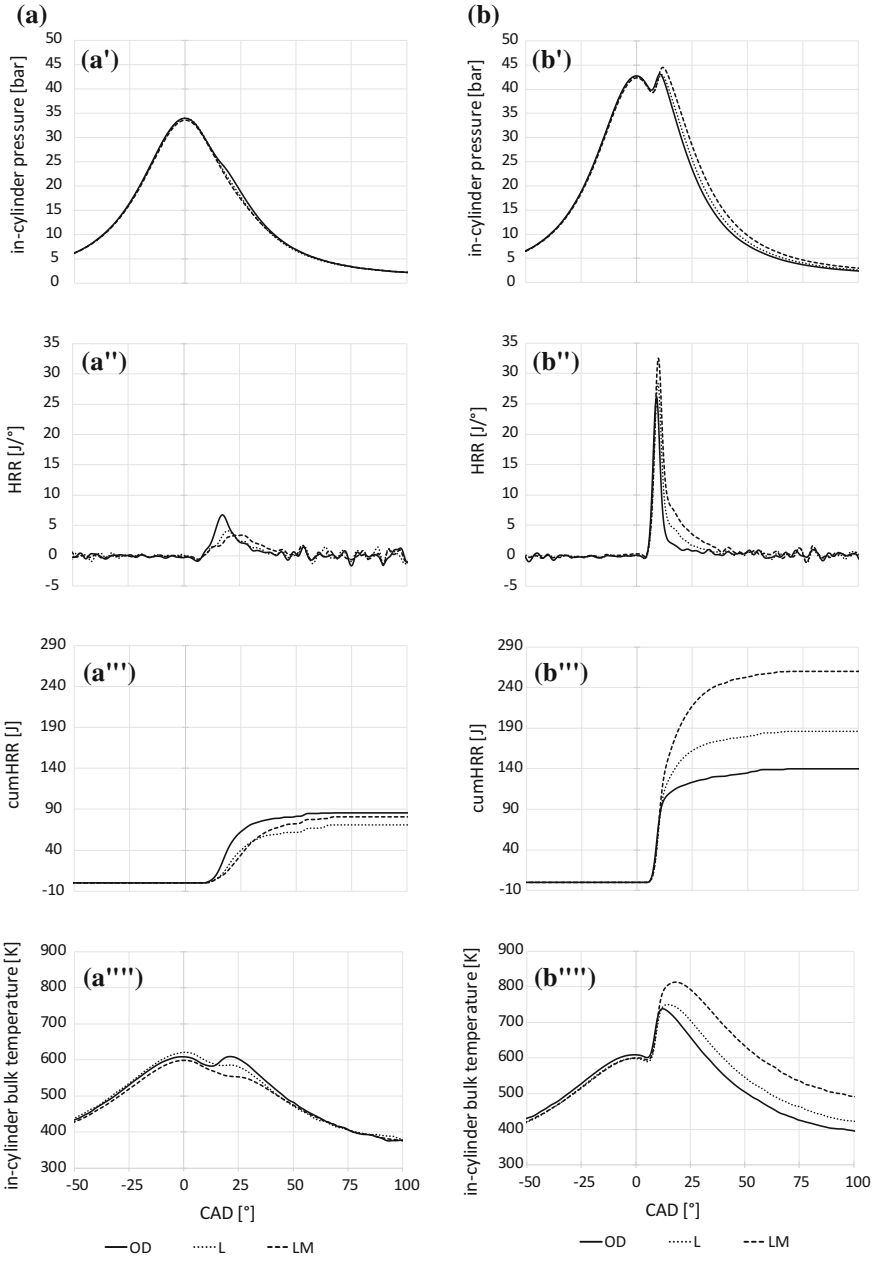

Fig. 10.11 Comparison of in-cylinder pressure, HRR, HRR cumulative, and in-cylinder bulk temperature for different methane rates at SOI = TDC (CR = 14, p_rail = 500 bar, ICP = 1.16 bar, column "a"; CR = 17, p_rail = 1250 bar, ICP = 1.16 bar, column "b")

applied and so a *p*-value was obtained, associated with each factor or combination of factors, for every output parameter. A low *p*-value means a high probability that a given output parameter is influenced by a specific factor (or combination of factors).

In Fig. 10.12a, *p*-values associated with each factor (CR, p_rail, SOI, ICP, G_{gas}) for each output parameter (IMEP, η_f, MPRR, THC, NO_x, CO) are plotted. It can be easily observed that SOI is the most influential factor, as p-value is very low for all output parameters. ICP is mainly influential on engine performance (IMEP, η_f, MPRR) and THC emissions, while G_{gas} is more influential on both engine performance (IMEP, η_f, MPRR) and engine emissions (THC, NO_x, CO). The less influential factor is p_rail, whose slight effect is visible only on NO_x emission levels.

In Table 10.4, the effect of the increase of each factor on each output parameter is reported. The symbol "↑" means that the output parameter increases as the corresponding input increases, while the symbol "↓" means that the output parameter decreases as the corresponding input increases. The symbol "=" associated with each of the previous symbols means that the effect is only slight. The two symbols together (as for SOI effect on IMEP and η_f) means that the trend was first increasing and then decreasing.

A more detailed analysis has been conducted performing the ANOVA for each level of G_{gas}: The question was whether the *p*-values associated with CR, p_rail, SOI, ICP shown in Fig. 10.12a could be confirmed for each level of G_{gas}, i.e., varying the engine load. The analysis, not reported here for brevity, did not highlight strong differences. However, a significant effect on CO and NO_x of the ICP as the methane flow rate increases and a significant effect of pilot injection pressure on indicated mean effective pressure and fuel conversion efficiency as the methane flow rate increases were observed.

Finally, observing Fig. 10.12b, the second-order most important effects can be recognized. If the injection pressure has the least first-order effect on the output parameters, the second-order effect in combination with pilot injection timing on engine performance (IMEP, η_f, MPRR) and THC emissions is significant, as well as the effect on NO_x emissions in combination with ICP. Another significant

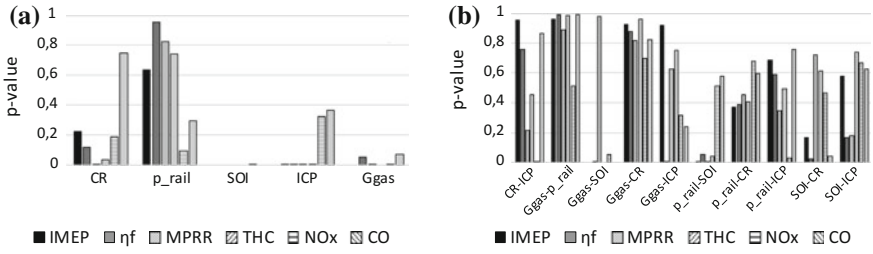

Fig. 10.12 *p*-value associated with each factor for each engine output parameter (plot "a"); *p*-value associated with second-order effects for each engine output parameter (plot "b")

Table 10.4 Trend determined by each factor on each engine output parameter

	IMEP	η_f	MPRR	THC	NO_x	CO
CR	↑	↑	↑	↓	↑	↓ =
p_rail	↓ =	↓ =	↓ =	↑	↑	↑
SOI	↑ ↓	↑ ↓	↓	↑	↓	↓
ICP	↑	↑	↑	↓	↓	↓
G_{gas}	↑	↓	↑	↑	↑	↓

second-order effect can be observed on η_f and CO emissions combining engine volumetric compression ratio and pilot injection timing.

10.5 Summary and Conclusions

In the first part of this work, a full factorial DoE has been performed on a single-cylinder diesel engine modified in order to operate in dual-fuel diesel–methane mode. The methane was fumigated along the intake duct thanks to an injector. During the experimental campaign, compression ratio, ICP, pilot injection timing and pressure, and methane flow rate were varied on several levels; this allowed to quantify the effect of each of them, as well as of their interaction, on combustion development, engine efficiency and pollutant levels at the exhaust. Results are summarized in the following:

- Pilot injection timing is the most influential factor on both engine performance and emissions. Very advanced or retarded timings (with respect to the tested range) showed potential in enabling PPCI thanks to the long ignition delay: in these conditions, very low emission levels and acceptable levels of maximum pressure rise rate with no or little penalization on fuel conversion efficiency were observed.
- Methane flow rate supplied to the engine is influential too on both engine performance and emissions; the fuel conversion efficiency and NO_x levels both increase as methane flow rate increases, while CO and THC levels have a more complicated behavior, increasing when methane flow rate increases from low to medium values, decreasing from medium to high values.
- ICP mainly influences engine performance; the effect of THC is stronger, while CO and NO_x are only marginally influenced. A more detailed analysis, specialized at different methane flow rates, highlighted a significant effect on CO and NO_x as the methane flow rate increases. Moreover, a higher value of ICP helped in reaching PPCI with very retarded pilot injection timing.
- Engine volumetric compression ratio influences significantly only maximum pressure rise rate and THC, reducing both of them; in combination with pilot injection timing, it influences also fuel conversion efficiency and CO emissions.
- Pilot injection pressure has the weakest first-order effect on both engine performance and emissions; a more detailed analysis, specialized at different

methane flow rates, highlighted a significant effect of pilot injection pressure on indicated mean effective pressure and fuel conversion efficiency as the methane flow rate increases. Moreover, its effect increases on engine performance and THC emissions in combination with pilot injection timing.

Summarizing, a proper choice of design and calibration is necessary to reach HCCI combustion in dual-fuel engines. Besides the broadly investigated strategy based on very advanced pilot injections, retarded injection timings, combined with high ICP, determine very low levels of nitrogen oxides and maximum pressure rise rate, with little or no penalty on engine efficiency and THC and CO levels. This strategy, already investigated in diesel combustion, showed very good combustion performance at low/medium load when combined with EGR (hot and cooled) and swirl. Therefore, an ad hoc experimental campaign shall be performed also for dual-fuel combustion with the aim of evaluating EGR and swirl effects, besides the already investigated injection pressure and engine compression ratio, on engine performance and emissions abatement.

Acknowledgements The authors wish to thank Mr. Adriano Romano for his fundamental contribution to the present work, in particular during the ANOVA of the experimental data.

References

Ansari E, Poorghasemi K, Khoshbakht Irdmousa B, Shahbakhti M et al (2016) Efficiency and emissions mapping of a light duty diesel—natural gas engine operating in conventional diesel and RCCI modes. SAE technical paper 2016-01-2309. https://doi.org/10.4271/2016-01-2309

Carlucci AP, de Risi A, Laforgia D, Naccarato F (2008) Experimental investigation and combustion analysis of a direct injection dual-fuel diesel–natural gas engine. Energy 33 (2):256–263. https://doi.org/10.1016/j.energy.2007.06.005

Carlucci A, Laforgia D, Saracino R (2009) Effects of in-cylinder bulk flow and methane supply strategies on charge stratification, combustion and emissions of a dual-fuel DI diesel engine. SAE technical paper 2009-01-0949. https://doi.org/10.4271/2009-01-0949

Carlucci A, Laforgia D, Saracino R, Toto G (2010) Study of combustion development in methane-diesel dual fuel engines, based on the analysis of in-cylinder luminance. SAE technical paper 2010-01-1297. https://doi.org/10.4271/2010-01-1297

Carlucci AP, Ficarella A, Laforgia D (2014) Potentialities of a common rail injection system for the control of dual fuel biodiesel-producer gas combustion and emissions. J Energ Eng 140(3). https://doi.org/10.1061/(ASCE)EY.1943-7897.0000150

Carlucci AP, Colangelo G, Ficarella A, Laforgia D, Strafella L (2015) Improvements in dual-fuel biodiesel-producer gas combustion at low load through pilot injection splitting. J Energ Eng 141(2):C4014006-1–C4014006-8. https://doi.org/10.1061/(ASCE)EY.1943-7897.0000231

Carlucci AP, Laforgia D, Ficarella A, Strafella L (2017) Improvement of a dual fuel biodiesel-producer gas engine performance acting on biodiesel injection parameters and strategy. Fuel 209:754–768. https://doi.org/10.1016/j.fuel.2017.07.100

Dahodwala M, Joshi S, Koehler E, Franke M (2014) Investigation of diesel and CNG combustion in a dual fuel regime and as an enabler to achieve RCCI combustion. SAE technical paper 2014-01-1308. https://doi.org/10.4271/2014-01-1308

Di Blasio G, Belgiorno G, Beatrice C (2017a) Effects on performances, emissions and particle size distributions of a dual fuel (methane-diesel) light-duty engine varying the compression ratio. Appl Energ 204:726–740. https://doi.org/10.1016/j.apenergy.2017.07.103

Di Blasio G, Belgiorno G, Beatrice C (2017b) Parametric analysis of compression ratio variation effects on thermodynamic, gaseous pollutant and particle emissions of a dual-fuel CH4-diesel light duty engine. SAE technical paper 2017-01-0764. https://doi.org/10.4271/2017-01-0764

Donateo T, Carlucci AP, Strafella L, Laforgia D (2014) Experimental validation of a CFD model and an optimization procedure for dual fuel engines. SAE world congress & exhibition 2014, Detroit (Michigan), 8–10 Apr 2014. SAE technical paper 2014-01-1314. https://doi.org/10.4271/2014-01-1314

Doosje, E, Willems F, Baert R (2014) Experimental demonstration of RCCI in heavy-duty engines using diesel and natural gas. SAE technical paper 2014-01-1318. https://doi.org/10.4271/2014-01-1318

Garcia P, Tunestal P (2015) Experimental investigation on CNG-diesel combustion modes under highly diluted conditions on a light duty diesel engine with focus on injection strategy. SAE Int J Engines 8(5):2177–2187. https://doi.org/10.4271/2015-24-2439

Gharehghani A, Hosseini R, Mirsalim M, Jazayeri SA, Yusaf T (2015) An experimental study on reactivity controlled compression ignition engine fueled with biodiesel/natural gas. Energy 89:558–567. https://doi.org/10.1016/j.energy.2015.06.014

Guerry ES, Raihan SM, Srinivasan KK, Krishnan SR, Sohail A (2016) Injection timing effects on partially premixed diesel–methane dual fuel low temperature combustion. Appl Energ 162:99–113. https://doi.org/10.1016/j.apenergy.2015.10.085

Hariprasad T (2013) Effect of injection pressure on performance of dual fuel diesel engines. SAE 2013-01-2887. doi.org/10.4271/2013-01-2887

Hasan MM, Rahman MM (2016) Homogeneous charge compression ignition combustion: advantages over compression ignition combustion, challenges and solutions. Renew Sust Energ Rev 57:282–291. https://doi.org/10.1016/j.rser.2015.12.157

He L, Lu Z, Zhang J, Geng L, Zhao H, Li X (2018) Low-carbon economic dispatch for electricity and natural gas systems considering carbon capture systems and power-to-gas. Appl Energ 224:357–370. https://doi.org/10.1016/j.apenergy.2018.04.119

Hosmath RS, Banapurmath NR, Khandal SV, Gaitonde VN, Basavarajappa YH, Yaliwal VS (2016) Effect of compression ratio, CNG flow rate and injection timing on the performance of dual fuel engine operated on Honge oil methyl ester (HOME) and compressed natural gas (CNG). Renew Energ 93:579–590. https://doi.org/10.1016/j.renene.2016.03.010

Ibrahim MM, Varuna Narasimhan J, Ramesh A (2015) Comparison of the predominantly premixed charge compression ignition and the dual fuel modes of operation with biogas and diesel as fuels. Energy 89:990–1000. https://doi.org/10.1016/j.energy.2015.06.033

Kimura S, Ogawa H, Matsui Y, Enomoto Y (1997) An experimental analysis of low-temperature and premixed combustion for simultaneous reduction of NO_x and particulate emissions in direct injection diesel engines. Int J Engine Res 3(4):249–259. https://doi.org/10.1243/146808702762230932

Kimura S, Aoki O, Kitahara Y, Aiyoshizawa E (2001) Ultra-clean combustion technology combining a low-temperature and premixed combustion concept for meeting future emission standards. SAE technical paper 2001-01-0200. https://doi.org/10.4271/2001-01-0200

McKennaa RC, Bchini Q, Weinand JM, Michaelis J, König S, Köppel W, Fichtner W (2018) The future role of power-to-gas in the energy transition: regional and local techno-economic analyses in Baden-Württemberg. Appl Energ 212:386–400. https://doi.org/10.1016/j.apenergy.2017.12.017

Muhammad IK, Tabassam Y, Muhammad IK, Muhammad F, Muhammad W (2016) Research progress in the development of natural gas as fuel for road vehicles: a bibliographic review (1991–2016). Renew Sust Energ Rev 66:702–741. https://doi.org/10.1016/j.rser.2016.08.041

Napolitano P, Guido C, Beatrice C, Del Giacomo N (2017) Application of a dual fuel diesel-CNG configuration in a Euro 5 automotive diesel engine. SAE technical paper 2017-01-0769. https://doi.org/10.4271/2017-01-0769

Nithyanandan K, Gao Y, Wu H, Lee C et al (2017) An optical investigation of multiple diesel injections in CNG/diesel. SAE technical paper 2017-01-0755. https://doi.org/10.4271/2017-01-0755 (Dual-fuel combustion in a light duty optical diesel engine. SAE technical paper 2017-01-0755 2017. https://doi.org/10.4271/2017-01-0755)

Ogawa H, Shibata G, Goto J, Jiang L (2016) Performance improvements in a natural gas dual fuel compression ignition engine with 250 MPa pilot injection of diesel fuel as an ignition source. SAE technical paper 2016-01-2306. https://doi.org/10.4271/2016-01-2306

Pali R, Amit D, Saroj KM (2018) Influence of gaseous fuel induction on the various engine characteristics of a dual fuel compression ignition engine: a review. Renew Sust Energ Rev 82:3333–3349. https://doi.org/10.1016/j.rser.2017.10.055

Paykani A, Kakaee A, Rahnama P, Reitz RD (2015) Effects of diesel injection strategy on natural gas/diesel reactivity controlled compression ignition combustion. Energy 90:814–826. https://doi.org/10.1016/j.energy.2015.07.112

Poorghasemi K, Saray R, Ansari E, Khoshbakht Irdmousa B, Shahbakhti M, Naber JD (2017) Effect of diesel injection strategies on natural gas/diesel RCCI combustion characteristics in a light duty diesel engine. Appl Energ 199:430–446. https://doi.org/10.1016/j.apenergy.2017.05.011

Raihan SM, Guerry ES, Dwivedi U, Srinivasan KK, Krishnan SR (2015) Experimental analysis of diesel-ignited methane dual-fuel low-temperature combustion in a single-cylinder diesel engine. J Energ Eng 141(2), C4014007 1–13. https://doi.org/10.1061/(ASCE)EY.1943-7897.0000235

Ryu K (2013a) Effects of pilot injection pressure on the combustion and emissions characteristics in a diesel engine using biodiesel–CNG dual fuel. Energ Convers Manage 76:506–516. https://doi.org/10.1016/j.enconman.2013.07.085

Ryu K (2013b) Effects of pilot injection timing on the combustion and emissions characteristics in a diesel engine using biodiesel-CNG dual fuel. Appl Energ 111:721–751. https://doi.org/10.1016/j.apenergy.2013.05.046

Song H, Liu C, Li Y, Wang Z, Chen L, He X, Wang J (2018) An exploration of utilizing low-pressure diesel injection for natural gas dual-fuel low-temperature combustion. Energy 153:248–255. https://doi.org/10.1016/j.energy.2018.04.041

Srinivasan KK, Krishnan SR, Midkiff KC (2006) Improving low load combustion, stability and emissions in pilot-ignited natural gas engines. Proc Inst Mech Eng D-J Auto 220(2):229–239. https://doi.org/10.1243/09544070JAUTO104

Wang B, Li T, Ge L, Ogawa H (2016) Optimization of combustion chamber geometry for natural gas engines with diesel micro-pilot-induced ignition. Energ Convers Manage 122:552–563. https://doi.org/10.1016/j.enconman.2016.06.027

Woschni G (1967) A universally applicable equation for the instantaneous heat transfer coefficient in the internal combustion engine. SAE technical paper 670937. https://doi.org/10.4271/670931

Xu M, Cheng W, Li Z, Zhang H, An T, Meng Z (2016a) Pre-injection strategy for pilot diesel compression ignition natural gas engine. Appl Energ 179:1185–1193. https://doi.org/10.1016/j.apenergy.2016.07.024

Xu M, Cheng W, Zhang H, An T, Zhang S (2016b) Effect of diesel pre-injection timing on combustion and emission characteristics of compression ignited natural gas engine. Energ Convers Manage 117:86–94. https://doi.org/10.1016/j.enconman.2016.02.054

Yang B, Xi C, Wei X, Zeng K, Lai MC (2015) Parametric investigation of natural gas port injection and diesel pilot injection on the combustion and emissions of a turbocharged common rail dual-fuel engine at low load. Appl Energ 143:130–137. https://doi.org/10.1016/j.apenergy.2015.01.037